

# 3D Two-Photon Microprinting of Nanoporous Architectures

Frederik Mayer,\* Daniel Ryklin, Irene Wacker, Ronald Curticean, Martin Čalkovský, Andreas Niemeyer, Zheqin Dong, Pavel A. Levkin, Dagmar Gerthsen, Rasmus R. Schröder, and Martin Wegener\*

A photoresist system for 3D two-photon microprinting is presented, which enables the printing of inherently nanoporous structures with mean pore sizes around 50 nm by means of self-organization on the nanoscale. A phase separation between polymerizable and chemically inert photoresist components leads to the formation of 3D co-continuous structures. Subsequent washing-out of the unpolymerized phase reveals the porous polymer structures. To characterize the volume properties of the printed structures, scanning electron microscopy images are recorded from ultramicrotome sections. In addition, the light-scattering properties of the 3D-printed material are analyzed. By adjusting the printing parameters, the porosity can be controlled during 3D printing. As an application example, a functioning miniaturized Ulbricht light-collection sphere is 3D printed and tested.

The idea of self-assembly is charming because certain types of 2D and 3D nanostructures can be manufactured in large volumes within short time. Along these lines, researchers have previously discussed a large variety of periodic as well as nonperiodic nanoporous architectures.<sup>[1,2]</sup> Similarly charming is the idea of 3D additive manufacturing.<sup>[3,4]</sup> Here, nearly arbitrary but well-defined complex 3D architectures are manufactured by directly converting digital information into physical objects, albeit often requiring longer times and exhibiting restrictions concerning the minimum achievable feature (or voxel) size.<sup>[5]</sup> Ideally, one could combine the best of these two worlds and use self-assembly for small spatial scales combined with controlled 3D manufacturing on a larger scale. Early steps in this direction have already been taken and photoresists for stereolithography that enable the printing of porous structures have been published. These

photoresists rely on a nonpolymerizable template phase that is introduced into the photoresist in a solid<sup>[6]</sup> or liquid<sup>[7]</sup> state and that is removed after polymerization.


Herein, we introduce a photoresist formulation for two-photon absorption-based 3D laser microprinting that allows combining the two approaches of self-assembly and additive manufacturing. Hereby, we realize 3D nanoporous architectures with pore sizes around 50 nm that require control ranging from the scale of ten nanometers to the millimeter scale, i.e., over nearly five orders of magnitude. We foresee applications of such structures in controlling diffuse light scattering, for example in terms of 3D-printed minia-

ture Ulbricht light-collection spheres, as nanoparticle filters in microfluidics, as super-hydrophobic surfaces, or as scaffolds for cell and tissue culture.

In 3D laser microprinting, one most important requirement regarding the photoresist is that it must neither be absorbing nor light scattering at the excitation wavelength used (often around 800 nm). In particular, if a porosity is introduced into a photoresist using a template, index matching between the monomers and the template is a necessity to avoid light scattering during the laser-writing process.<sup>[6,7]</sup> A different, well-known approach for the creation of inherently nanoporous polymers in the bulk is polymerization-induced phase separation.<sup>[1]</sup> Applications include chromatographic separation media<sup>[8]</sup> and superhydrophobic surfaces.<sup>[9]</sup> Polymerization-induced phase separation has already been employed for the 3D printing of

F. Mayer, D. Ryklin, Dr. I. Wacker, R. Curticean, M. Čalkovský, A. Niemeyer, Prof. P. A. Levkin, Prof. D. Gerthsen, Prof. R. R. Schröder, Prof. M. Wegener  
3DMM2O–Cluster of Excellence (EXC-2082/1-390761711)  
Karlsruhe Institute of Technology (KIT)  
Karlsruhe 76131, Germany  
E-mail: Frederik.Mayer@kit.edu; martin.wegener@kit.edu

F. Mayer, A. Niemeyer, Prof. M. Wegener  
Institute of Applied Physics (APH)  
Karlsruhe Institute of Technology (KIT)  
Karlsruhe 76128, Germany

 The ORCID identification number(s) for the author(s) of this article can be found under <https://doi.org/10.1002/adma.202002044>.

© 2020 The Authors. Published by WILEY-VCH Verlag GmbH & Co. KGaA, Weinheim. This is an open access article under the terms of the Creative Commons Attribution License, which permits use, distribution and reproduction in any medium, provided the original work is properly cited.

DOI: 10.1002/adma.202002044

F. Mayer, A. Niemeyer, Prof. M. Wegener  
Institute of Nanotechnology (INT)  
Karlsruhe Institute of Technology (KIT)  
Karlsruhe 76128, Germany

D. Ryklin, Dr. I. Wacker, R. Curticean, Prof. R. R. Schröder  
Centre for Advanced Materials  
Ruprecht-Karls-Universität Heidelberg  
Im Neuenheimer Feld 225, Heidelberg 69120, Germany

M. Čalkovský, Prof. D. Gerthsen  
Laboratorium für Elektronenmikroskopie  
Karlsruhe Institute of Technology (KIT)  
Karlsruhe 76128, Germany

Dr. Z. Dong, Prof. P. A. Levkin  
Institute of Biological and Chemical Systems-Functional Molecular Systems (IBCS-FMS)  
Karlsruhe Institute of Technology (KIT)  
Eggenstein-Leopoldshafen 76344, Germany

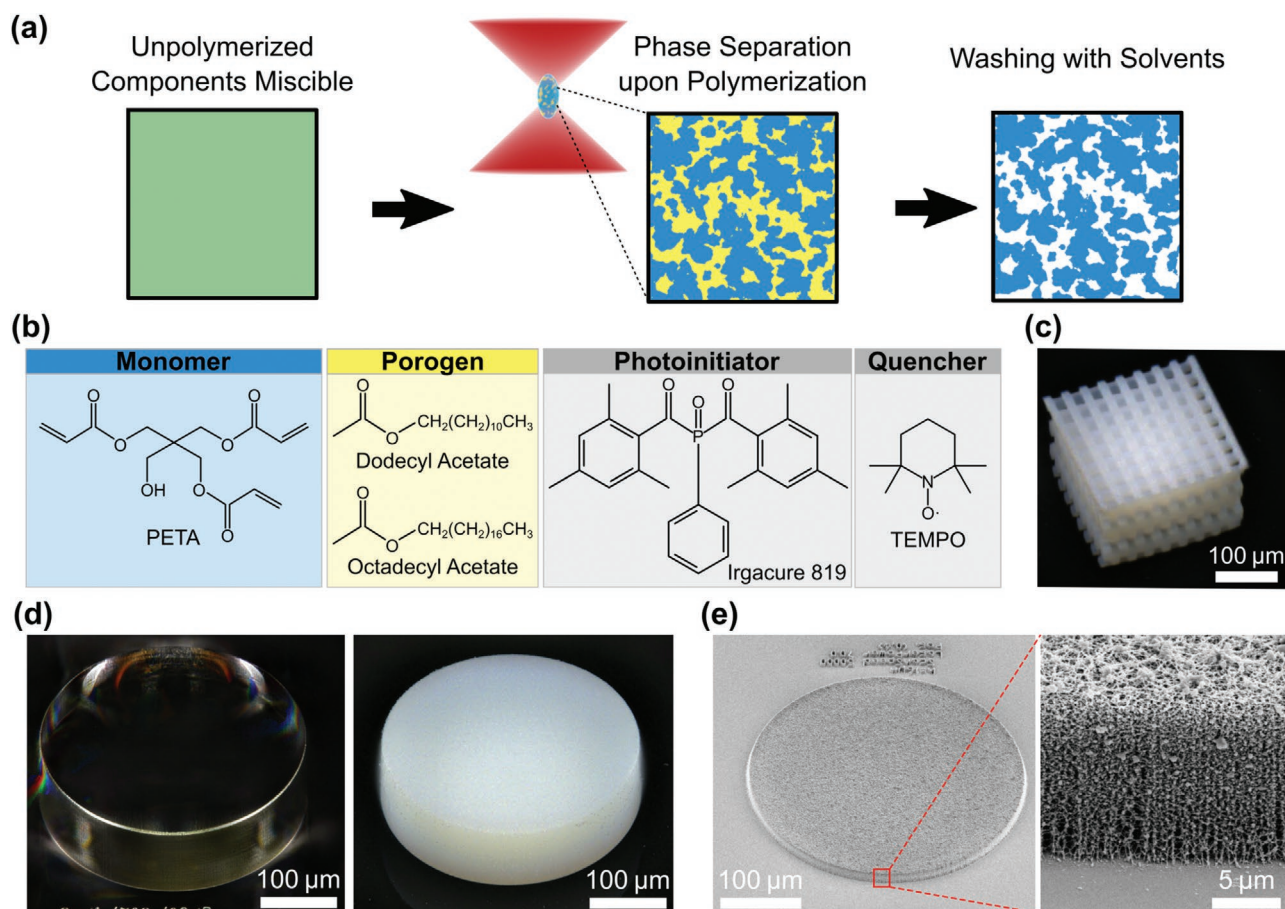


**Figure 1.** a) In polymerization-induced phase separation, a demixing between polymer and porogens (e.g., organic solvents) occurs upon polymerization. Thus, a porous polymer with porogens in the pores is formed. In two-photon 3D laser microprinting, polymerization is triggered optically via nonlinear excitation in the laser focus. After writing, unpolymerized material is washed out from the porous polymer using organic solvents, and the pores are filled with air after drying. b) Components of the photoresist. c) Optical microscopy image of an example 3D woodpile structure (rod spacing  $a = 30 \mu\text{m}$ ). d) Cylinders ( $350 \mu\text{m}$  diameter and  $100 \mu\text{m}$  height) printed out of a “conventional” (Nanoscribe IP-S, left-hand side) photoresist and our phase-separating resist. Due to strong light scattering in the nanoporous cylinder (right), it appears white, whereas the solid cylinder (left) has a transparent appearance. e) SEM images taken on a gold-sputtered ( $10 \text{ nm}$  thickness) sample.

glass structures using stereolithography.<sup>[10]</sup> Here, co-continuous structures consisting of a polymer phase and a glass-precursor phase are printed. Porous and nonporous glass structures are obtained by subsequent thermal treatment. Our work is distinct from that work in that we demonstrate a photoresist for two-photon absorption-based 3D laser microprinting, which allows for better spatial resolution than stereolithography. Furthermore, we are 3D printing porous polymer structures instead of porous glass structures.

Following the approach of polymerization-induced phase separation, we have developed a photoresist for 3D laser microprinting. The underlying principle is illustrated in **Figure 1a**. The components of our photoresist are summarized in **Figure 1b**. The polymerization mixture mainly consists of monomers and porogens (commonly organic solvents) that are miscible in the unpolymerized state. This implies that the unpolymerized mixture also exhibits a homogeneous refractive-index distribution throughout the volume. Therefore, light scattering, which would hinder 3D laser lithography, is not present in the unpolymerized state. In contrast, if a polymerization reaction is triggered and the polymer chains start to grow, the reaction will eventually

reach a degree of polymerization where a separation between the porogen and the polymer phases occurs. For a given monomer, the choice of the porogen is therefore crucial for the occurrence of this process. The type of porogen determines the scale of the porous structure.<sup>[1]</sup> With respect to our photoresists, we aim for pore sizes that lie well below typical lithography voxel sizes (i.e., below  $\approx 200 \text{ nm}$ ). After polymerization (i.e., after 3D printing of the sample), we develop our samples in acetone for 30 min in order to wash out the porogen and the unpolymerized photoresist from the pores. To preserve the pores from collapsing, we employ supercritical drying. Subsequently, the pores are filled with air. As the refractive-index contrast between air and polymer is significant, pronounced light scattering occurs. When leaving out the supercritical drying step, we observe significant shape distortions and pronounced shrinkage. In contrast, when employing supercritical drying, we observe no significant shape distortions, and shrinkage is comparable to that of pure pentaerythritol triacrylate (PETA)-based photoresists. To demonstrate the 3D capability of the photoresist, we show an optical microscopy image (reflection mode with ring illumination) of a 3D example structure in **Figure 1c**. The full width of the square-shaped rods is  $15 \mu\text{m}$ .

The text in Figure 1e has a linewidth of about 1  $\mu\text{m}$ . Likewise, to demonstrate the difference in light scattering of structures printed out of a “conventional” photoresist (Nanoscribe IP-S) and the phase-separating photoresist presented here, corresponding cylinders (350  $\mu\text{m}$  diameter and 100  $\mu\text{m}$  height) are depicted next to each other in Figure 1d. The porous cylinder appears homogeneously white, as opposed to the optically clear appearance of the “conventional” cylinder. Typical scanning electron microscopy (SEM) images recorded from a gold-coated (10 nm thickness) and otherwise unprocessed porous cylinder are depicted in Figure 1e. From all SEM images taken, we conclude that the scale of the porosity at the structure’s surface lies in the deep sub-micrometer regime, but we do not yet gain any knowledge about the substructure within the volume. To investigate this aspect, we cut ultramicrotome sections of our 3D-printed samples that are imaged in the SEM detecting back-scattered electrons.

In fact, a close examination of the homogeneity of the porosity throughout the volume of our structures was crucial during the testing phase of our resist. In the beginning, we typically 3D printed structures from our phase-separating resist under ambient conditions. In doing so, we observed a strong decrease in porosity toward the center of printed cylinders (350  $\mu\text{m}$  diameter and 100  $\mu\text{m}$  height), which we could trace back to the formation of an oxygen depletion zone toward the

center of the cylinders (not depicted). Oxygen is known to be a radical quencher and therefore strongly affects the polymerization kinetics.<sup>[11,12]</sup> We thus remove oxygen from the photoresist prior to printing our samples by exposing it to a nitrogen atmosphere. To suppress uncontrolled polymerization and thus to avoid a strong deterioration of the spatial 3D printing resolution, we added the radical scavenger 2,2,6,6-tetramethylpiperidinyloxy (TEMPO) to the photoresist. Indeed, in our photoresists containing TEMPO instead of oxygen, we are able to 3D print complex structures with very homogeneous porosity. The 3D woodpile crystal shown in Figure 1c is a benchmark example. A different example exhibiting finer features is shown in Figure S4 (Supporting Information). We estimate a spatial resolution of a couple of micrometers (see 3D-printed text in Figure 1e). However, one should expect a proximity effect that is more pronounced than in standard nonporous photoresists.

In Figure 2a, we present SEM images recorded from ultramicrotome sections of our samples. For this purpose, the porous polymer structures have been stained with osmium tetroxide to increase material contrast for imaging with back-scattered electrons. Thereafter, the samples have been infiltrated with Epon resin. Thus, the light-gray regions represent the polymer and the darker regions correspond to Epon. Due to the finite penetration depth of the electron beam into the thin (80 nm) ultramicrotome

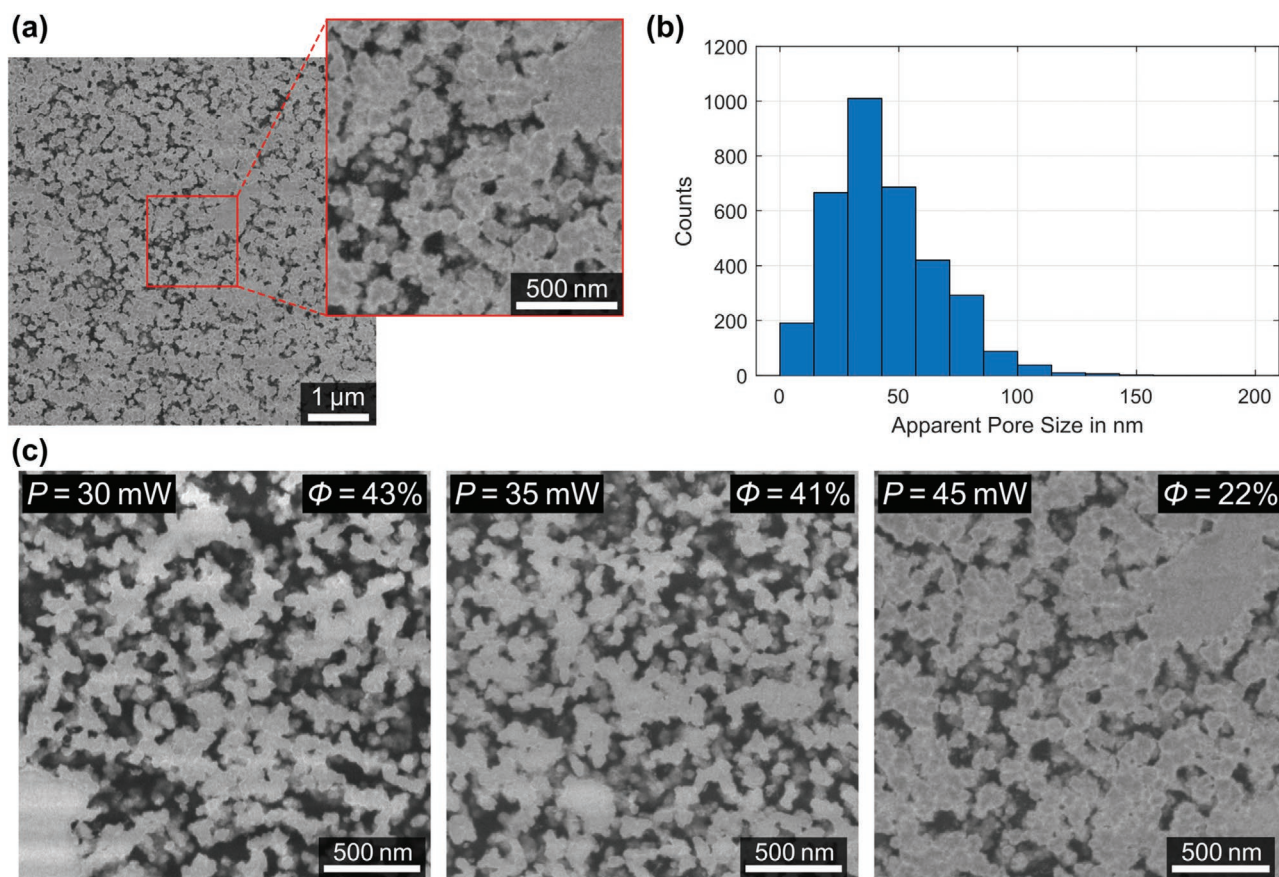


**Figure 2.** a) Example of an SEM image recorded from an ultramicrotome section. The light gray regions represent the osmium-stained polymer, whereas the dark regions correspond to the filled-in Epon epoxy resin. Polymer particles below the surface of the Epon matrix exhibit an intermediate gray value. b) Apparent 2D pore size distribution extracted from the 2D microscopy images. c) Ultramicrotomy SEM images recorded from samples written with varying writing power. For increasing writing power, the porosity  $\phi$  decreases.

sections, regions with intermediate brightness values are visible as well. They represent polymer particles that are not in direct contact with the top surface of the section. In Figure 2b, we plot the distribution of effective pore sizes which has been extracted from the 2D example image in (a) using an algorithm based on the Euclidean distance transform (for details see the Supporting Information).<sup>[13]</sup> The extraction of the pore size from 2D rather than 3D images results in a systematic error, which we do not correct for in terms of a stereological correction. The porosity,  $\phi$ , amounts to  $\phi = 22\%$  in this case, which we have obtained by setting a threshold following Otsu's method<sup>[14]</sup> and by subsequent averaging the resulting binary image. SEM images taken on sections from cylinders that have been 3D printed with three different laser powers are depicted in Figure 2c. For increasing

laser power from 30 to 45 mW, we observe a decrease in porosity from 43% to 22%—evidencing that in situ control of the porosity during writing is possible. This is an interesting finding, since the volume fraction of the nonpolymerizable progen, which makes up about 54% of the volume of the photoresist, should naively determine the degree of porosity. A possible explanation is that—in 3D laser microprinting in contrast to bulk polymerization—only small voxels on a sub-micrometer scale are polymerized sequentially. Thus, it is well conceivable that the diffusion length of the monomer on the timescale of polymerization lies in the regime of the voxel size. This interpretation is consistent with the fact that low-porosity structures can be obtained by multiple exposures (cf. Figure 3). Here, the monomer has sufficient time to diffuse into the pores.

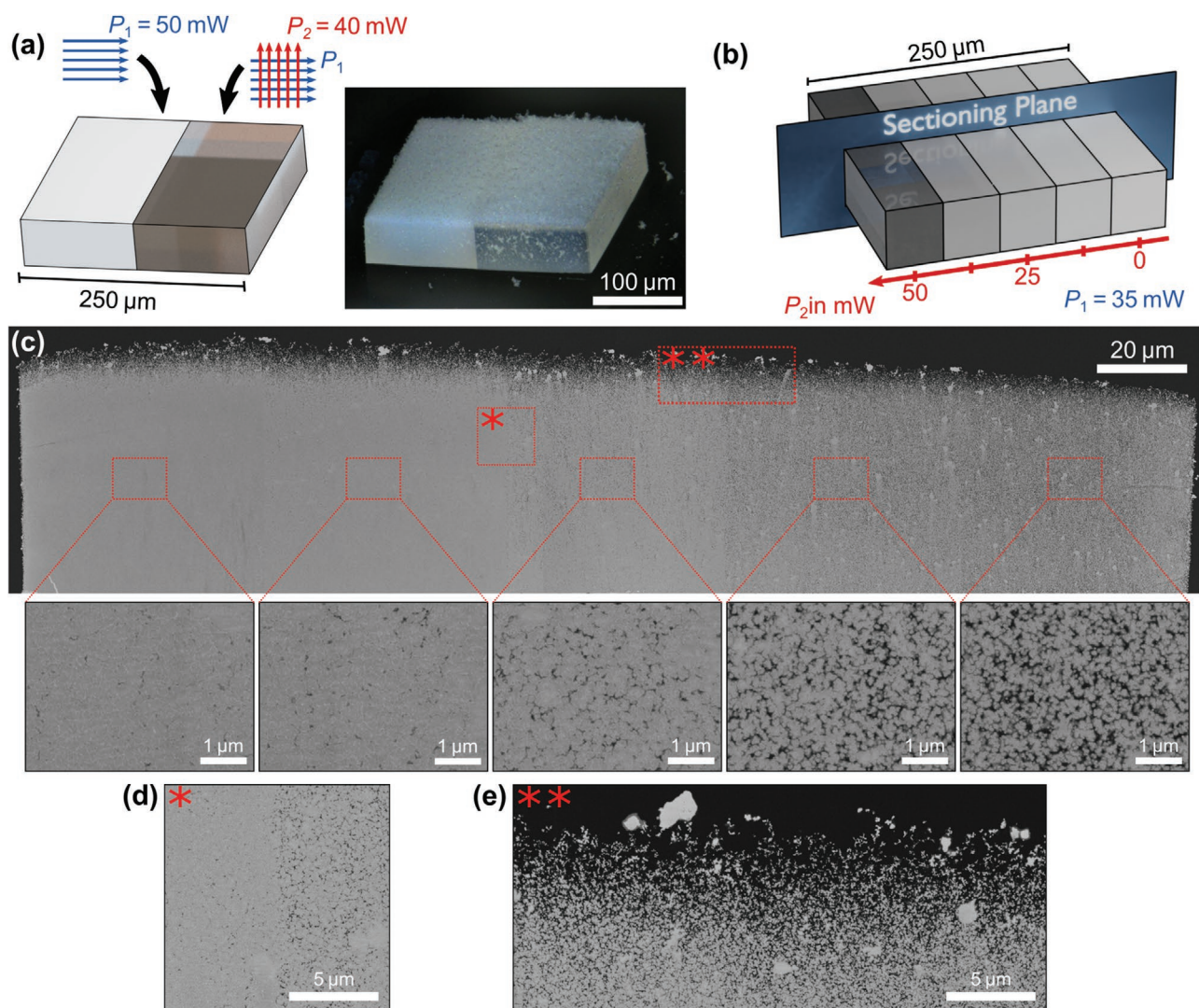


**Figure 3.** To increase the exposure dose, we employ a writing strategy in which each layer is exposed twice. a) Demonstration block where the right-hand side is exposed twice, whereas the left-hand side is exposed once for reference. The right-hand side becomes transparent, whereas the left-hand side is homogeneously light scattering. b) Sketch of the sample 3D printed for subsequent ultramicrotomy and SEM imaging. At fixed scanning speed and at fixed exposure power  $P_1 = 35$  mW, the exposure power  $P_2$  is varied throughout the structure. The sectioning plane for ultramicrotomy is indicated in blue. c) SEM image of ultramicrotome section of the structure from (b). Insets show magnified views of all regions written with different exposure conditions. The porosity decreases for increasing power  $P_2$ . d) Magnified view of the transition between two regions with different exposure power  $P_2$ . The transition in porosity is remarkably sharp. e) Magnified top view of the structure. Due to dose accumulation during writing, we typically observe a “snow-like” film with low porosity on top of all structures.

As the results on the variation of the exposure power are promising, we aim for decreasing the porosity even further. In the limit of zero porosity, light scattering should vanish, giving the structures a transparent appearance. Unfortunately, increasing the exposure dose by increasing the laser power is not an option because of limited available laser power. Decreasing the focus speed and thereby decreasing the 3D printing speed is not an attractive option either. Therefore, we apply a double-exposure writing strategy. Results are shown in Figure 3. In Figure 3a, each layer of the structure is exposed by an optical exposure power  $P_1$  in a first writing step, and with an exposure power  $P_2$  in a subsequent second exposure step. On the right-hand side of Figure 3a, we show an optical microscopy image of a block for which the left half has only seen a single exposure of the writing laser, whereas the right-hand side has been exposed twice. Indeed, the right-hand side has a transparent appearance in the volume, indicating a different porous substructure. To investigate this finding in more detail, we have written a set of blocks in which we vary the second exposure power  $P_2$ , and inspect ultramicrotome sections as indicated in Figure 3b. In this fashion, we examine and visualize the dependence on the second exposure power in a single sample. In Figure 3c, an SEM image of such a section is shown at the top. Insets in this image are highlighted by the small red rectangles. As anticipated from the above experiments, we observe a reduction in porosity from 27% to 3% with increasing power  $P_2$ . In Figure 3d, we show a magnified view of

a transition region between different porosities. The transition is remarkably sharp and takes place on a sub-micrometer scale. Figure 3e displays a zoom-in into the top surface of our printed structure: We observe a gradual decrease in porosity over a length scale of about  $5\ \mu\text{m}$  on top of the structures, which we attribute to unintentional dose accumulation. This effect leads to a thin light-scattering layer on top of the 3D-printed structures. Such a layer is also visible on top of the structure displayed in Figure 3a.

As a second method for characterizing the volumetric properties of our samples, we perform optical measurements of the light-scattering coefficient  $\mu_s$ . This quantity is the inverse of the optical scattering mean free path  $l_s = \mu_s^{-1}$ . It can be determined by measuring the ballistic transmission  $I(z)/I_0$  through samples of defined thickness  $z$ , following Beer-Lambert's law  $I(z)/I_0 = \exp(-\mu_s z)$  (see the Supporting Information). Measurements of the scattering coefficient  $\mu_s$  of the volume of the samples manufactured by using a single- and double-exposure writing strategy, respectively, taken at a free-space wavelength of  $\lambda = 561\ \text{nm}$ , are plotted in Figure 4a,b, respectively. In Figure 4b, to allow for a direct comparison, we additionally plot the porosity determined from SEM images. Qualitatively, we observe a decreasing light-scattering coefficient with increasing exposure dose in both cases starting from  $\mu_s \approx 0.16\ \mu\text{m}^{-1}$ , which translates to a scattering mean free path of  $l_s \approx 6\ \mu\text{m}$ . For the double-exposed samples, as to be expected from the measurements of the porosity (Figure 4b),

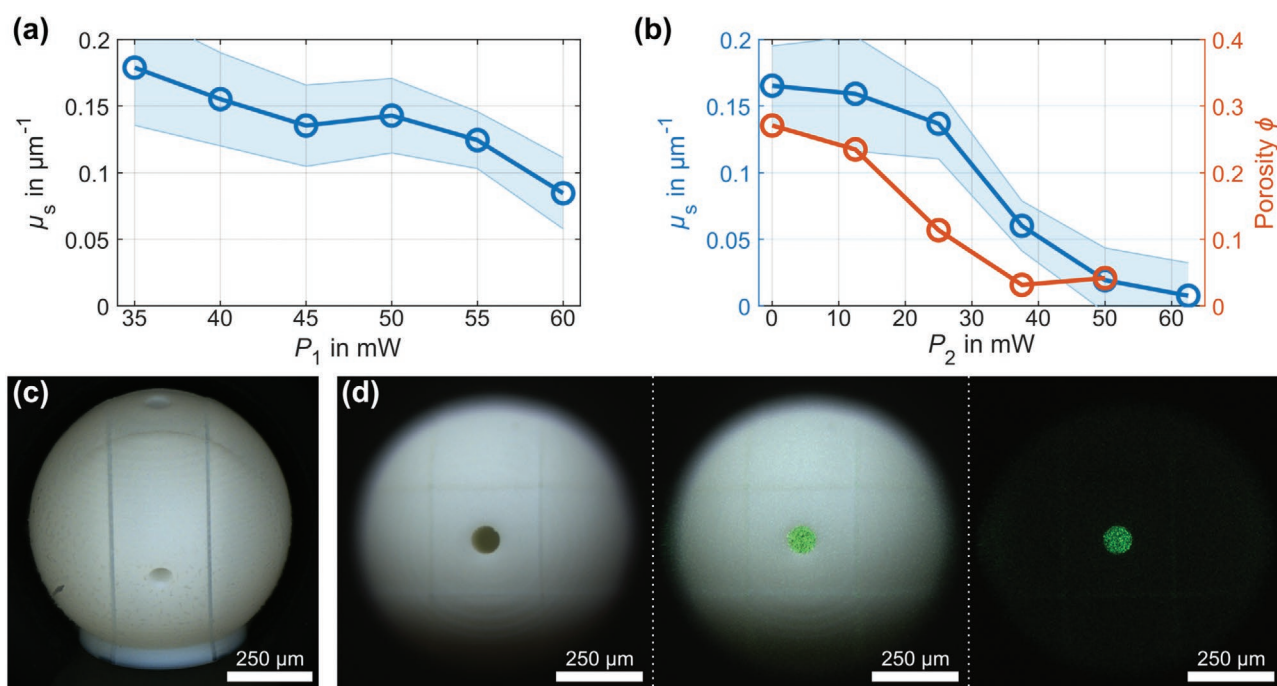


**Figure 4.** Experiments on light scattering in porous polymer structures. a) The light scattering coefficient (at 561 nm wavelength) decreases with increasing exposure power. The shaded regions indicate 95% confidence intervals. b) Using a double-exposure writing scheme (compare Figure 3a), the scattering coefficient can be tuned over a wide range, and light scattering vanishes for high exposure doses. The exposure power of the first exposure is held constant at  $P_1 = 35\ \text{mW}$ , while the power  $P_2$  is varied. The porosity, extracted from SEM images on ultramicrotome sections, evolves accordingly. c) Oblique view of a miniaturized 3D-printed Ulbricht integrating sphere, making use of the high diffuse reflectivity of the optically thick light-scattering porous walls. d) Demonstration of a functioning miniature 3D-printed light-integrating sphere. Top-view optical microscopy image under white-light illumination (left), green light ( $\lambda = 532\ \text{nm}$ ) emerging from the top hole while illuminating the side hole by a laser (right), and composite image (middle). Note that little if any green light leaks through the walls of the light-integrating sphere.

this decrease is by far more pronounced and  $\mu_s$  converges toward zero.

The direct 3D micrometer-scale printing of light-scattering structures offers new applications. For example, conceptually, with increasing thickness of a strongly light-scattering layer, its diffuse reflectivity ideally approaches unity. As a demonstration of this property we have 3D printed a miniaturized Ulbricht light-integrating sphere, an oblique view of which is depicted in Figure 4c. This Ulbricht sphere has an outer diameter of 800  $\mu\text{m}$ , an inner diameter of 400  $\mu\text{m}$ , and two circular holes with 80  $\mu\text{m}$  diameter each, one at the top and one on the side. In Figure 4d, we show the results of experiments demonstrating the functionality of the Ulbricht sphere. Here, we focus a laser beam ( $\lambda = 532 \text{ nm}$ ) into the hole at the side of the sphere and switch off white-light illumination, while observing the sphere from the top (right panel). Under these conditions, we observe laser light emerging from the top hole, while the walls of the Ulbricht sphere appear dark, evidencing that almost no light is transmitted through them. Overall, this example is a good indication that the diffuse reflectivity of the walls is sufficient to perform meaningful measurements.

In summary, we have, for the first time, developed a photoresist for 3D two-photon microprinting that can be used for the manufacturing of inherently nanoporous polymer microstructures with mean pore sizes around 50 nm. For a detailed investigation of the substructure within the volume of the 3D-printed architectures, we have taken SEM images on ultramicrotome sections. We have shown that we can tune the porosity of the printed material over a wide range by tuning the writing parameters. Experiments on the light-scattering properties of 3D-printed structures show good agreement with the porosity. Finally, we have demonstrated a miniaturized 3D-printed Ulbricht light-integrating sphere as an early application example.

## Experimental Section

**Laser Microprinting:** 3D printing was performed using a commercial apparatus (Photonic Professional GT, Nanoscribe GmbH) with a 25 $\times$ /NA 0.8 objective lens (Zeiss LCI Plan-Neofluar 25 $\times$ /0.8) in the dip-in mode. All structures shown were printed with a focus velocity of 5  $\text{cm s}^{-1}$ , a slicing distance of 1  $\mu\text{m}$ , and a hatching distance of 0.5  $\mu\text{m}$ . During printing, the samples were held under a chemically inert nitrogen atmosphere. In addition, each printing job was started by printing dummy structures to further deplete oxygen in the photoresist droplet (ten cylinders with 350  $\mu\text{m}$  diameter and 100  $\mu\text{m}$  height). The exposure power for these dummy cylinders was 50 mW.

**Supercritical Drying:** After 3D printing, the samples were developed by immersing them in acetone for 30 min. Subsequently, supercritical drying was performed using a commercial device (Leica EM CPD300). In the process, the sample was transferred to the instrument's chamber and cooled to 14  $^{\circ}\text{C}$ . Afterward, the acetone in the chamber was replaced by liquid carbon dioxide by repeatedly flushing with liquid carbon dioxide and releasing the acetone. The chamber was then heated above the critical point of carbon dioxide to 40  $^{\circ}\text{C}$  while keeping the pressure below 100 bar. Finally, all carbon dioxide was slowly released from the chamber. The entire drying process took about 60 min.

**Photoresist Composition:** The photoresist consisted of (mass fractions) pentaerythritol triacrylate 52.94% (PETA, Sigma-Aldrich), irgacure 819 2.12%, 2,2,6,6-tetramethylpiperidinyloxy 0.07% (TEMPO, Sigma-Aldrich), dodecyl acetate 22.43% (Sigma-Aldrich), and octadecyl

acetate 22.43% (TCI Chemicals). All components were added to a flask and treated in an ultrasonic bath for half an hour until a homogenous mixture was obtained. Before writing, the photoresist was bubbled with nitrogen gas to remove oxygen.

**Sample Preparation and Ultramicrotomy:** Samples were incubated for 24 h with 2%  $\text{OsO}_4$  in acetone, infiltrated for 3 h with 50% Epon in acetone, embedded in 100% Epon (42.4 g glycid ether 100, 29.6 g DDSA, 18.4 g MNA, and 2.4 g BDMA, all from SERVA), and polymerized at 60  $^{\circ}\text{C}$  for 2 days. Ultrathin (80 nm) sections were cut from trimmed resin blocks and placed on pieces of silicon wafer.

**Electron Microscopy:** Sections were imaged in a field-emission scanning electron microscope (Ultra 55, Carl Zeiss Microscopy) at 1.5 keV primary electron energy using the ESB detector for back-scattered electrons and the Atlas 5 software for automated recording of large scan fields.

## Supporting Information

Supporting Information is available from the Wiley Online Library or from the author.

## Acknowledgements

This work was funded by the Deutsche Forschungsgemeinschaft (DFG, German Research Foundation) under Germany's Excellence Strategy 2082/1-390761711 (Excellence Cluster "3D Matter Made to Order") and by the priority program DFG-SPP 1839. The authors acknowledge support by the Helmholtz program Science and Technology of Nanosystems (STN), the Karlsruhe School of Optics and Photonics (KSOP), the ERC Starting Grant (337077-DropCellArray), and the Carl Zeiss Foundation. R.R.S. acknowledges funding from the BMBF under Grant No. 13N14476.

## Conflict of Interest

The authors declare no conflict of interest.

## Keywords

3D two-photon microprinting, light scattering, photoresists, porous materials, ultramicrotomy

Received: March 24, 2020

Revised: May 11, 2020

Published online: June 30, 2020

- [1] F. Svec, *J. Chromatogr. A* **2010**, 1217, 902.
- [2] Z. Alothman, *Materials* **2012**, 5, 2874.
- [3] T. Baldacchini, *Three-Dimensional Microfabrication Using Two-Photon Polymerization: Fundamentals, Technology, and Applications*, William Andrew, Norwich, NY, USA **2016**.
- [4] I. Gibson, D. Rosen, B. Stucker, *Additive Manufacturing Technologies: 3D Printing, Rapid Prototyping, and Direct Digital Manufacturing*, Springer, Berlin, Germany **2015**.
- [5] V. Hahn, P. Kiefer, T. Frenzel, J. Qu, E. Blasco, C. Barner-Kowollik, M. Wegener, *Adv. Funct. Mater.* **2020**, 30, 1907795.
- [6] X. Mu, T. Bertron, C. Dunn, H. Qiao, J. Wu, Z. Zhao, C. Saldana, H. J. Qi, *Mater. Horiz.* **2017**, 4, 442.
- [7] D. W. Johnson, C. Sherborne, M. P. Didsbury, C. Pateman, N. R. Cameron, F. Claeysens, *Adv. Mater.* **2013**, 25, 3178.

- [8] F. Svec, J. M. J. Fréchet, *Chem. Mater.* **1995**, *7*, 707.
- [9] P. A. Levkin, F. Svec, J. M. J. Fréchet, *Adv. Funct. Mater.* **2009**, *19*, 1993.
- [10] D. G. Moore, L. Barbera, K. Masania, A. R. Studart, *Nat. Mater.* **2020**, *19*, 212.
- [11] J. B. Mueller, J. Fischer, F. Mayer, M. Kadic, M. Wegener, *Adv. Mater.* **2014**, *26*, 6566.
- [12] L. Yang, A. Münchinger, M. Kadic, V. Hahn, F. Mayer, E. Blasco, C. Barner-Kowollik, M. Wegener, *Adv. Opt. Mater.* **2019**, *7*, 1901040.
- [13] M. Ender, J. Joos, T. Carraro, E. Ivers-Tiffée, *J. Electrochem. Soc.* **2012**, *159*, A972.
- [14] N. Otsu, *IEEE Trans. Syst. Man Cybern.* **1979**, *9*, 62.